Annals of the BMVA Vol. 2013, No. 5, pp 1–15 (2013)

Statistical region based active contour using a fractional entropy descriptor: Application to nuclei cell segmentation in confocal microscopy images

A. Histace[1], L. Meziou[1], B. J. Matuszewski[2], F. Precioso[3], M. F. Murphy[4], F. Carreiras[5]

[1] ETIS UMR CNRS 8051, University of Cergy-Pontoise, ENSEA, Cergy, France
[2] ADSIP Research Centre, University of Central Lancashire, Preston, UK
[3] I3S - UMR CNRS 6070, University of Nice/Sophia-Antipolis, Nice, France
[4] Liverpool John Moores University, Liverpool, UK
[5] ERRMECe, University of Cergy-Pontoise, Cergy, France
⟨aymeric.histace@u-cergy.fr⟩

Abstract

We propose an unsupervised statistical region based active contour approach integrating an original fractional entropy measure for image segmentation with a particular application to single channel actin tagged fluorescence confocal microscopy image segmentation. Following description of statistical based active contour segmentation and the mathematical definition of the proposed fractional entropy descriptor, we demonstrate comparative segmentation results between the proposed approach and standard Shannon's entropy on synthetic and natural images. We also show that the proposed unsupervised statistical based approach, integrating the fractional entropy measure, leads to very satisfactory segmentation of the cell nuclei from which shape characterization can be calculated.

1 Introduction

Segmentation of cellular structures is an essential tool in cell microscopic imaging as it enables measurements to be made of sub-cellular organization and has the potential to help understand the internal architecture of cells and how this alters with disease and therapy. More specifically, the work presented in this paper has been carried out to help us analyze

changes to the actin cytoskeleton following sub-lethal doses of ionizing radiation insult. As actin is key to providing cells with structural and mechanical integrity then being able to quantify changes to its organization could help us to better understand the mechanical properties of cells and how these change through radiation insult. Therefore the final goal of this research effort is to better understand the bio-mechanical responses of cells during radiation therapy. In this context, we propose an unsupervised segmentation approach of fluorescence confocal microscopy images which represents practical computational problem when considering many monolayer acquisitions – in order to effectively extract nuclei as a first step for providing spatial reference frame for analyzing cytoskeleton changes.

To date, only few methods have been proposed to address direct segmentation (without any denoising preprocessing of acquired images) of cell structures in fluorescence confocal microscopy images. In former approaches proposed in [Ortiz De Solorzano et al., 1999] and [Sarti et al., 2000], authors focused on nuclei segmentations. In [Yan et al., 2008], authors proposed cell segmentation in 2D-fluorescent images with two channels (actin and nucleus tagging) using a multiphase level-set combining Chan-Vese [Chan and Vese, 2001] and geodesic active contour models, together with repulsive force introduced to prevent segmented cells from overlapping. In [Mosaliganti et al., 2009, Zanella et al., 2010] automated 3D cell segmentation from a 3D confocal acquisition of early Zebrafish embriogenesis is proposed; Two different fluorescent markers (red for nuclei and green for membrane) are used to easily discriminate nuclei from cell membranes. In [Zanella et al., 2010], authors introduced an adapted version of the subjective surface technique [Sarti et al., 2002] for surface reconstruction from missing boundary information whereas [Mosaliganti et al., 2009] use a multiphase level-set based on probability correlation functions.

Within a level set framework as in [Yan et al., 2008, Mosaliganti et al., 2009], our method aims at a different objective: segmentation of 2D microscopy images extracted from a single channel confocal acquisition with only one fluorescent marker used for actin tagging. Due to a highly complex actin appearance, a high level of noise and a strong non-homogeneity of intensity and gradient information, the segmentation of cell structures in such imaging data, is a very challenging task. Moreover, a particular attention is given to completely avoid any enhancement preprocessing [Pop et al., 2011] and to reduce to its minimum, manual interventions during the whole segmentation process. Part of this work was presented at the 2012 MIUA conference [Meziou et al., 2012b]. This paper is an extended version of the MIUA paper with detailed explanation added to each section.

The remainder of this article is organized as follows: in Section 2, the data used in the experiment are described briefly; in Section 3, the framework of histogram based active contour using entropy estimation is recalled and the proposed Rényi-like measure is introduced with the complete derivation of the corresponding governing PDE steering the evolution of the contour. Section 4 focuses on experiments on synthetic and natural images, and Section 5 reports the results obtained for microscopy images followed by conclusions drawn in Section 6.

2 Fluorescence confocal microscopy images

The data used in this paper were obtained from human prostate cells (PNT2). Actin were labelled with phalloidin-FITC and all imaging was carried out using a Zeiss LSM510 confocal microscope. Fig. 1 shows different slices from the microconfocal acquisition of the mono-

Annals of the BMVA Vol. 2013, No. 5, pp 1–15 (2013)

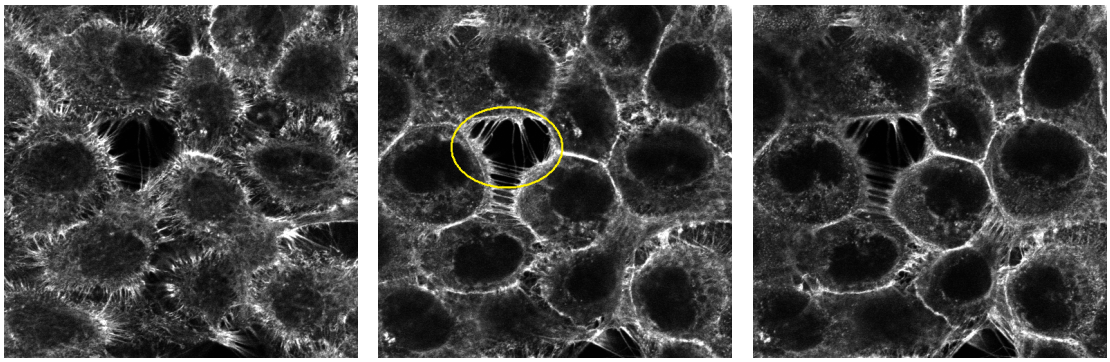

(a) (b) (c)

Figure 1: Examples of actin tagged fluorescence confocal microscopy images extracted from a 3D microconfocal acquisition of the monolayer PNT2 cell culture. (a) Lower slice (with low z-stack index), (b) Mid-slice with the lowest level of structural noise (a "hole" is highlighted in yellow which should not to be confused with a nucleus), (c) Upper slice with non-homogeneity of the fluorescent marker on the left hand side.

layer PNT2 cell culture. The stack volume is defined on the $512 \times 512 \times 98$ grid of pixels each $0.21\mu m \times 0.21\mu m \times 0.11\mu m$ in size [Matuszewski et al., 2011].

The choice of filamentous marker actin (F-actin) is motivated by the fact that F-actin is known to play a vital role in in cell structure and mechanics [Hall, 2009]. As Actin is one of the main existing proteins in human cytoskeleton, studying its changes and properties could help to understand better cell bio-mechanical properties. As actin is mostly present in the cytoplasm, we can notice that high intensities in slices of Fig. 1 show areas of high concentration of actin in proximity of cell membrane which allows us to find approximate location of cell boundaries whereas darkest areas represent nuclei. Due to the high level of Poisson noise corrupting these images and their particular textured structures, it is difficult to propose a parametric model of this. Moreover, due to the particular texture of actin, classic region based active contour approach, like the Chan and Vese one [Chan and Vese, 2001], fails even in segmenting properly the boundaries of nuclei corresponding to each cell [Meziou et al., 2011]: We then propose to tackle this segmentation using statistical based active contour (see [Lecellier et al., 2010] for an overview on the work on this area) more adapted to this particular context than classic region based ones.

3 Active contour segmentation using a fractional entropy descriptor

3.1 Statistical region based active contours

Originally proposed in [Kass et al., 1988], the basic idea of the active contour is to iteratively evolve an initial curve towards the boundaries of target objects driven by the combination of internal forces, determined by the geometry of the evolving curve, and external forces, induced from the image. Image segmentation methods using active contour are often derived from a variational principle in which a functional defined on contours encodes our

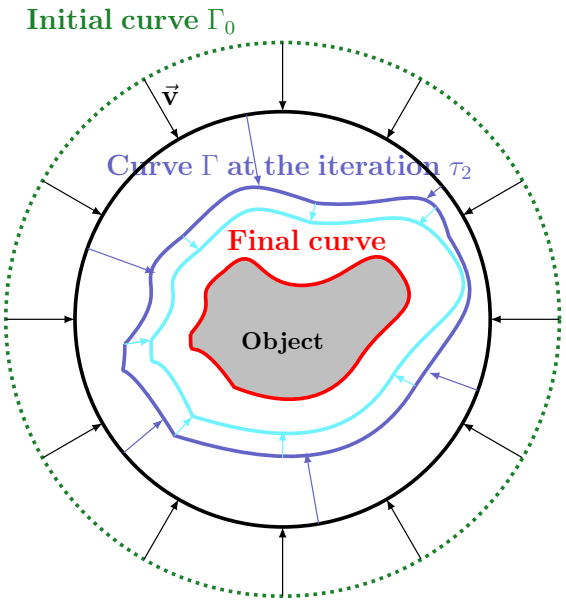

Figure 2: Illustration of active contour segmentation: $\Gamma = \Gamma(p, \tau)$ denotes the coordinate of the point p of the curve at iteration τ of the segmentation process.

knowledge about desirable solutions. The functional minimization leads to a partial differential equation (PDE), constructed as the Gateaux derivative gradient flow which steers the evolution of the active contour.

Formerly introduced in [Aubert et al., 2003], statistical region based active contour methods are derived from traditional region based approaches [Jehan-Besson et al., 2003] by utilizing integral statistics as descriptors of the inner (Ω_{in}) and outer (Ω_{out}) regions delimited by the active curve Γ at a given iteration τ of the segmentation process (see Fig. 2 for illustration). In the following, we recall main theoretical aspects of entropy based active contour. For more details, refer to [Herbulot et al., 2006, Lecellier et al., 2010, Meziou et al., 2012a].

First, let $H(\Omega_i)$ denote an integral entropy estimation associated to a particular region Ω_i within image such as

$$H(\Omega_i) = \int_{\Omega_i} \varphi\left(\hat{p}(\mathbf{I}(\mathbf{x}), \Omega_i)\right) \, d\mathbf{x} \,, \tag{1}$$

with φ a monotonically increasing function, $\mathbf{I}(\mathbf{x})$ the luminance of pixel $\mathbf{x} = (x, y)$ and $\hat{p}$ the non-parametrically estimated Probability Density Function (PDF) of region Ω_i, estimated using Parzen window technique:

$$\hat{p}(\mathbf{I}(\mathbf{x}), \Omega_i) = \frac{1}{|\Omega_i|} \int_{\Omega_i} G_\sigma(\mathbf{I}(\mathbf{x}) - I(\lambda)) \, d\lambda, \tag{2}$$

where $\lambda \in [0...2^n - 1]$, n is the quantization level of image intensity function, and G_σ is the Gaussian kernel of standard deviation σ. In the framework of statistical region based active contour segmentation, corresponding functional H_T to be minimized is defined as a competition between inner and outer regions characterized by the introduced, in Eq (1),

entropy descriptor H:

$$H_T = H(\Omega_{in}) + H(\Omega_{out}) + g\int_\Gamma ds, \tag{3}$$

where g is a positive real value and s standard arclength of the curve. This functional combines measures of the considered entropy descriptor of inner Ω_{in} and outer Ω_{out} regions of the curve with an additional regularization term minimizing the curve length. The Euler derivative of Eq. (3) and usual minimization scheme leads to the Partial Differential Equation (PDE) steering the evolution in the orthogonal direction $\mathbf{N}$ of the active curve Γ [Herbulot et al., 2006]:

$$\frac{\partial\Gamma}{\partial\tau} = \big(A(s,\Omega_{in}) + \varphi(p(\mathbf{I}(s),\Omega_{in})) - A(s,\Omega_{out}) + \varphi(p(\mathbf{I}(s),\Omega_{out})) + g\big)\mathbf{N} \tag{4}$$

where $s = \Gamma(p,\tau)$ and A is related to the proposed descriptor and is defined by:

$$A(s,\Omega_i) = -\frac{1}{|\Omega_i|}\int_{\Omega_i}\varphi'(\hat{p}(\mathbf{I}(\mathbf{x}),\Omega_i))[\hat{p}(\mathbf{I}(\mathbf{x}),\Omega_i) - G_\sigma(\mathbf{I}(\mathbf{x}) - \mathbf{I}(s))]\,d\mathbf{x}\,. \tag{5}$$

For illustration, let's consider the particular case of Shannon's entropy: φ function is given by

$$\varphi(r) = -r \times log(r)\,, \tag{6}$$

and then

$$H(\Omega_i) = -\int_{\Omega_i}\hat{p}(\mathbf{I}(\mathbf{x}),\Omega_i)log(\hat{p}(\mathbf{I}(\mathbf{x}),\Omega_i))d\mathbf{x}. \tag{7}$$

3.2 Fractional entropy descriptor

As it will be shown in the Experiments and results section, standard Shannon's entropy has some limitations in terms of segmentation performance: more specifically, this measure makes segmentation of corrupted (with Gaussian or Poissan noises) textured images challenging [Herbulot et al., 2006], and in the case of high level of structural noise, the segmentation results are not that satisfactory.

First of all, as shown in [Jehan-Besson et al., 2003], this can be explained by the fact that Shannon's criterion is equivalent to a region based approach depending only on variance difference in PDF_{in} and PDF_{out} regions. As a consequence if the corresponding PDFs cannot be discriminated by their second order statistics, this criterion is not applicable. Moreover, Shannon's entropy assumes that the corrupting noise (and then the corresponding PDF $\hat{p}$) can be parametrically modeled within the exponential family [Lecellier et al., 2010] which is not true when considering confocal microscopy data for instance. In this particular context, fractional entropy like the Rényi's entropy, proposed by [Rényi, 1960]:

$$H_R(\Omega_i) = \frac{1}{1-\alpha}log\int_{\Omega_i}\hat{p}(\mathbf{I}(\mathbf{x}),\Omega_i)^\alpha\,d\mathbf{x}\,. \tag{8}$$

It can be shown [Bromiley et al., 2004], using L'Hôpital, in the limit $\alpha \to 1$ Renyi's entropy converges to the Shannon's entropy. For any value of $\alpha \geq 0$, Rényi's entropy is nonnegative and for $\alpha \in [0,1]$, Rényi's entropy is concave and shows an additional parameter α which can be used to make it more or less sensitive to the shape of PDF $\hat{p}$. For illustration, Fig. 3

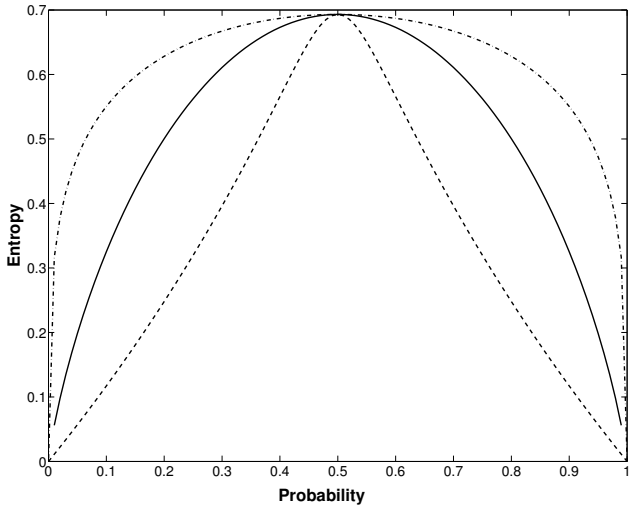

Figure 3: Rényi entropy H_R of Eq. (8) as a function of the probability p of a binary source $(p, 1-p)$ (Bernoulli's distribution), for three values of the order $\alpha = 0.4$ (dash-dotted line), $\alpha = 10$ (dashed line), and $\alpha = 1$ identified by plain line corresponding to the Shannon's entropy.

shows the Rényi's entropy of Eq. (8) considering the usual Bernoulli's distribution for input variable.

This relaxation property (see $\alpha = 0.4$ in Fig. 3) is the starting point of this proposed study. Unfortunately, Rényi's entropy as expressed in Eq. (8) is part of the non-integral entropy family that can not be easily associated to a region-based criterion in a classic active contour based segmentation. Nevertheless, taking benefits of the possible sensibility tuning of the Rényi's entropy using α parameter, we propose to define a fractional entropy measure adapted to the framework of statistical region-based active contour segmentation. For this, let consider Eq. (1) with φ function and its derivative given by:

$$\varphi(r) = \varphi_\alpha(r) = -log\,(r^\alpha) \text{ and } \varphi'_\alpha(r) = -\frac{\alpha}{r}\,. \tag{9}$$

with $\alpha \in [0, 1]$ Considering φ_α function of Eq. (9), we obtain an integral entropic measure[1] integrating a fractional parameter allowing some relaxation properties as shown Fig. 4. Moreover, let's note that at the limit $\alpha = 1$, we obtain $\varphi_\alpha(r) = -ln(\hat{p})$ which is the Ahmad-Lin estimator of Shannon's entropy [Ahmad and Lin, 1976].

[1]It should be noticed that as for the Renyi's entropy, the proposed entropy fulfills only two out of three conditions for the measure of amount of information as postulated by Shannon, and therefore the proposed entropy should not be confused with the Shannon entropy

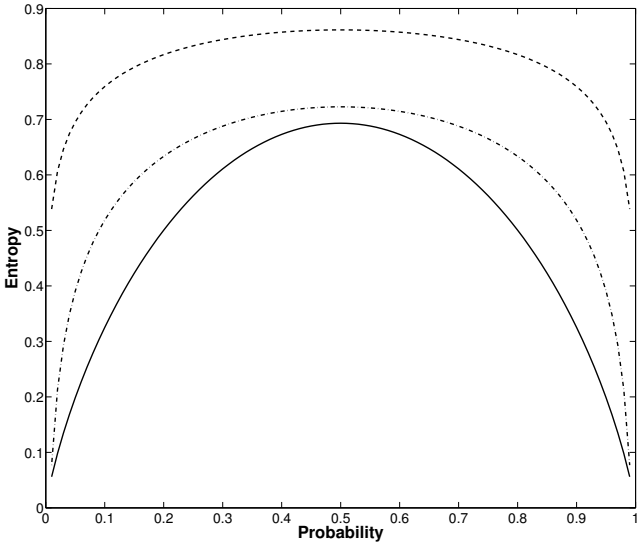

Figure 4: fractional entropy measure of Eq. (9) as a function of the probability p of a binary source $(p, 1-p)$ (Bernoulli's law), for two values of the order $\alpha = 0.1$ (dash-dotted line), $\alpha = 0.2$ (dashed line). Plain line corresponds to the Shannon's entropy.

4 Experiments and results

4.1 Numerical implementation

In order to be able to segment images presenting more than one target object, we propose to embed the segmentation process within the usual level-set framework [Osher and Sethian, 1988, Chan and Vese, 2001]. In this framework, considering the standard level-set embedding function $U : \Re^2 \times \Re^+ \to \Re$ and the evolution equation given by Eq. (4) with φ_α of Eq. (9), the following evolution PDE is obtained:

$$U^{k+1} = U^k + \Delta t \Big[\beta \nabla \cdot \left(\frac{\nabla U^{k+1/2}}{|\nabla U^{k+1/2}|} \right) - \begin{array}{l} \big(A^k(s,\Omega_{in}) + \varphi(p^k(\mathbf{I}(s),\Omega_{in}))\big) \\ -\big(A^k(s,\Omega_{out}) + \varphi(p^k(\mathbf{I}(s),\Omega_{out}))\big)\big) \Big], \end{array}$$

where $U^{k+1/2} = U^k - \Delta t \left(A^k(s,\Omega_{in}) + \varphi(p^k(\mathbf{I}(s),\Omega_{in}))\right) - \big(A^k(s,\Omega_{out}) + \varphi(p^k(\mathbf{I}(s),\Omega_{out}))\big)\big)$, and β is a weighting parameter.

For all experiments, the initialization of the active contour function U is a set of small circles uniformly distributed all over image which allows an easy initialization of the algorithm. Classic AOS (Additive Operator Splitting) scheme [Weickert et al., 1998] is used for implementation in order to obtain a reasonably fast convergence.

4.2 Synthetic data

In order to compare performances of both Shannon's entropy and the proposed fractional entropy measure inspired by Rényi's entropy, tests were carried out first on synthetic images.

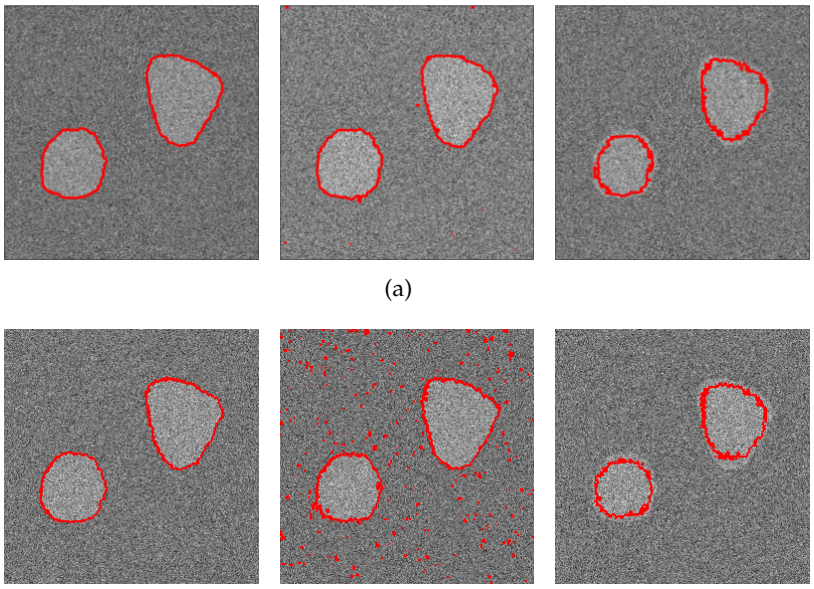

Figure 5: Segmentation of synthetic images (PSNR = 3dB) corrupted with different type of noise, and for different value of α parameter. (a) Zero-Mean Gaussian noise, (b) Poissan noise. From left to right : (a) $\alpha = 0.5$, $\alpha = 0.7$ and Shannon's entropy. For these experiments, the regularization term g is set to 5 ; (b) $\alpha = 0.1$, $\alpha = 0.5$ and Shannon's entropy. For these experiments, the regularization term g is set to 0.1.

For the first experiments, the main idea is to compare performances of the two aforementioned criteria with respect to the type of corrupting noise. zero-mean Gaussian and Poisson were considered with a related PSNR equal to 3 dB corresponding to significant level of image distortion. In order to also test capabilities of the proposed approach in terms of adaptation to topological changes, the considered synthetic images presents two disjoint objects to be segmented (see Fig. 5 for illustration).

Fig. 5 shows comparative segmentation results between the Rényi-like entropic measure and the standard Shannon's entropy. When Gaussian noise is considered, one can notice in Fig. 5.(a) that the proposed Renyi like entropic region descriptor leads to good segmentation results, whereas the Shannon criteria is less accurate even if the main structure is captured. This can be explained by the fact that Shannon's criterion is not statistically discriminative enough for high level of noise in the considered PDF when foreground and background have the same variance. Having in focus the proposed application to microscopic images corrupted by Poissan noise, Fig. 5.(b) shows results obtained for that kind of corrupting noise. Same global results are obtained than with Gaussian noise, even if it can be noticed that the α value leading to the satisfying segmentation is lower than for Gaussian noise.

Considering the proposed criterion, the robustness to the level of corrupting noise can be explained by the use of logarithm function combined with fractional values of α (α between 0 and 1) which can be interpreted here as a smoothing term on the shape of the PDF. As one can seen in Fig. 5, the more α tends to the asymtotic value of 1, the more the segmentation method is sensitive to the level of corrupting noise which is not that surprising considering the fact that for $\alpha = 1$ the corresponding entropy is the Shannon's entropy.

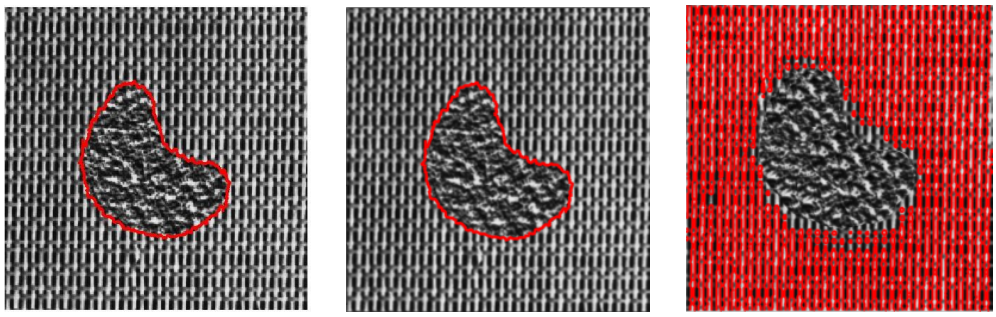

Figure 6: Segmentation of synthetic textured images with $\alpha = 0.5$ (left), 0.7 (middle) and Shannon entropy based segmentation.

The second experiment proposed consists in estimating the capability of the proposed method to discriminate between two regions having statistically similar characteristics. To illustrate this, we propose to segment the peanut shape in Fig. 6 which is characterized by a challenging statistical texture discrimination between PDF_{in} and PDF_{out} because of the similarity in the statistical distribution extracted from histograms of corresponding regions ((variance and mean of each PDF are very close even if visually each texture is quite different).

Fig. 6 shows results obtained with the Rényi-like criterion (for two different values of α) and the segmentation obtained with the standard Shannon's entropy. This latter descriptor completely failed in the segmentation task, whereas the proposed fractional entropy criterion leads to satisfying segmentation results for the two proposed values of α: it seems that the opportunity to take into account not only first order statistics of the PDF via α parameter tuning makes possible to dissociate similar distribution PDF_{in} and PDF_{out}.

4.3 Natural image segmentation

In this section, we present some segmentation results obtained on natural images. Fig. 7 shows comparative results for a flower image. This segmentation task is not the most challenging since the main part of the flower is statistically quite different from the background. Nevertheless, it remains a good reference in order to study the influence of parameter α related to the proposed fractional entropy descriptor. As it can be noticed in Fig. 7, Shannon's entropy criterion, for a same tuning of the regularization term g, leads to a global shape segmentation, whereas the proposed fractional entropy descriptor offers an additional flexibility of segmentation related to the α value: For instance, Fig. 7.(a) shows that for $\alpha = 0.1$, a better recall can be achieved than in Fig. 7.(d). Figs. 7.(b) and (c) show that a more detailed segmentation could also be obtained depending on the objective of the segmentation task.

Considering now a more challenging problem, we propose to tackle the segmentation of the "Cheetah" image. Fig. 8 shows comparative results obtained for different values of α parameter and for Shannon's entropy.

Obtained segmentation with Shannon's entropy criterion appears quite sensitive to noise and if the whole body of the animal is segmented, some background area are also included within the final result which is not that satisfying. When utilizing the proposed fractional entropy criterion, it can be noticed that better results are obtained. Once again, depending

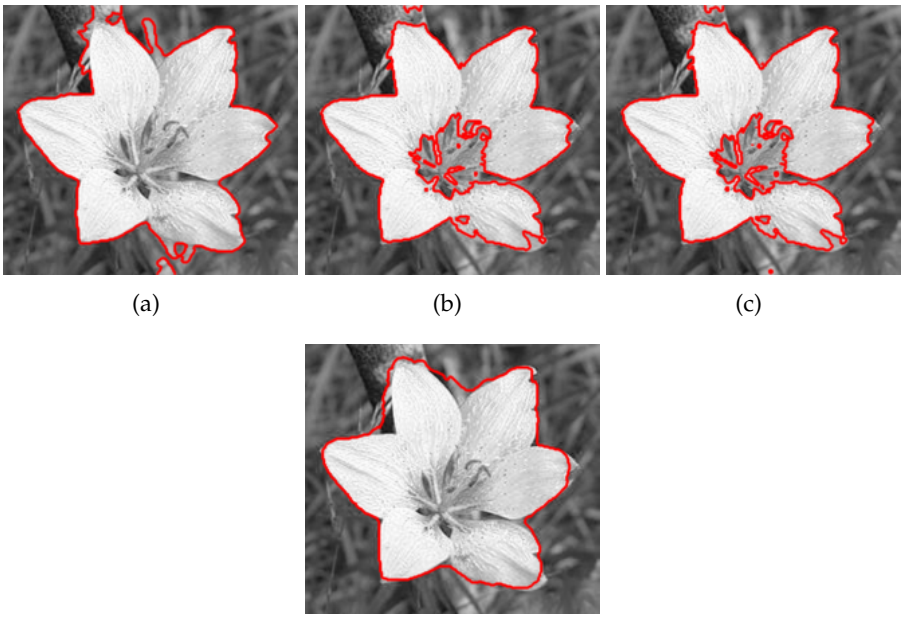

(a) (b) (c)

(d)

Figure 7: Different segmentation results of the "Flower image" using the proposed fractional entropy criterium: (a) $\alpha = 0.2$, (b) $\alpha = 0.4$, (c) $\alpha = 0.6$. (d) Shannon entropy based segmentation. For each experiment, g is set to 0.1.

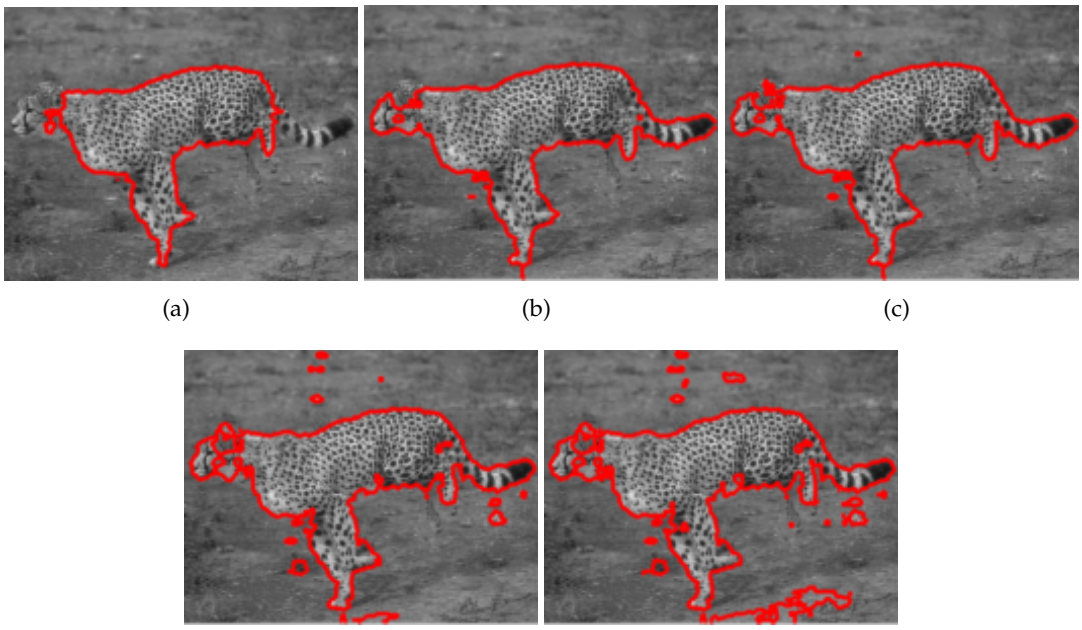

(a) (b) (c)

(d) (e)

Figure 8: Different segmentation results of the "Cheetah image" using the proposed fractional entropy criterium: (a) $\alpha = 0.1$, (b) $\alpha = 0.2$, (c) $\alpha = 0.3$. (d) Shannon entropy based segmentation. For each experiment, g is set to 0.3.

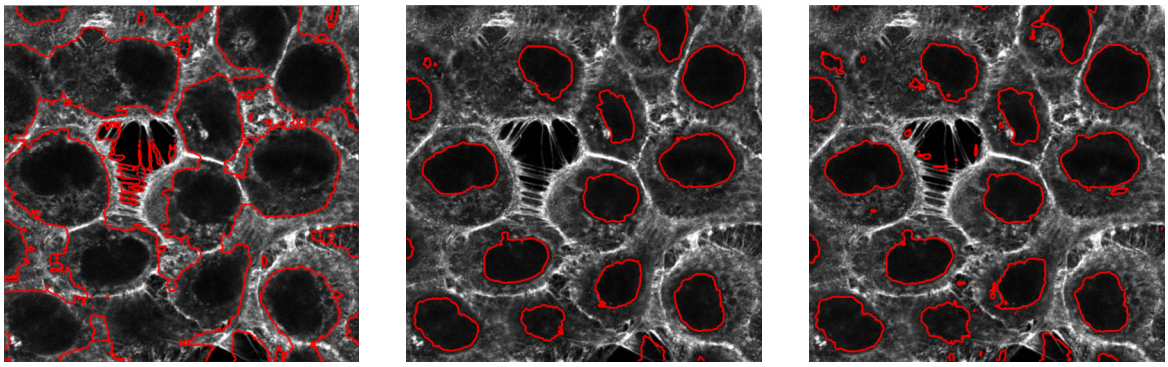

Figure 9: Comparative results of nuclei segmentation. Left: Shannon's entropy ; Middle and Right: Fractional entropy descriptor with $\alpha = 0.5$ (middle) and $\alpha = 0.7$ (right) ; for all experiments $g = 10$.

on the value of α parameter, different level of segmentation details are obtained: For $\alpha = 0.1$, only the main textured body of the cheetah is segmented whereas for upper values, the whole shape (including head and tail) is delineated. As illustrated with synthetic images, it also appears that the closer α is to one, the segmentation is sensitive to the background noise. This is not surprising since, as we have already mentioned it, for $\alpha = 1$, the proposed fractional entropy is related to the Ahmad-Lin estimator of Shannon's entropy.

5 Nuclei segmentation in confocal microscopy images

In this section, comparative segmentation results obtained are first described for the unsupervised nuclei segmentation within the mid-slice of the considered single channel confocal microscopy acquisition (Fig. 1(b)).

Fig. 9 shows results obtained with the standard Shannon's entropy criterion and the proposed fractional entropy descriptor. Considering experiments based on Shannon's entropy (Fig. 9 (left)), as one can notice, the method does not lead to satisfying results . Fig. 9 (middle and right) shows results of nuclei segmentation on the same slice, but with the proposed fractional entropy criterion: the nuclei segmentation is definitely improved. As one can notice, as actin is a complex structure, some artifacts could appear. It is possible to overcome this drawback with an adapted choice of α parameter. As one can see in Fig. 9, for $\alpha = 0.5$, smaller number of artifacts related to α value and those results show that this parameter plays an important role in the sensitivity of the criterion to the level of corrupting noise. Moreover, it is important to notice that the proposed fractional entropy measure can also distinguish a hole from a nucleus (which method based on Shannon's criterion was not able to achieve), whereas the associate PDFs are statistically very similar. This is in accordance with the results obtained on the highly corrupted synthetic images: When looking at the histogram of one of the considered microcopy images (see Fig. 10), it appears that the modes corresponding to the hole and to the nucleus class of the pixels are very close one to each other. As a consequence, as seen before, the Shannon's entropy is not able to discriminate both and finally, nuclei and hole are merged into a single class. Considering the fractional entropy descriptor, the related ability to separate very close PDF, makes possible the discrimination between both modes.

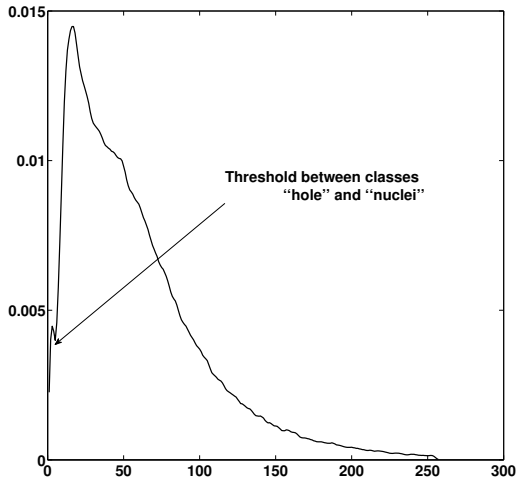

Figure 10: PDF of the mid-slice microscopy acquisition sequence.

Fig. 11 shows some segmentation results obtained on the whole stack of acquired images. Results shown are obtained with $\alpha = 0.5$, and $g = 10$. To obtain these results, a propagation initialization strategy, starting on middle slice is used which makes integration of some spatial coherence within the segmentation scheme to avoid propagation of false detection due to complex appearance of actin.

These results have been qualitatively considered as very satisfactory from an expert point of view and a very good start for further investigations on that particular data.

Finally, Fig. 12, shows results obtained on other images extracted from different acquisitions in order to illustrate the adaptability of the proposed process.

Results obtained remain satisfactory considering the fact that the non-homogeneity of the fluorescent actin marker significantly different than in previous images.

6 Conclusion

The contribution of the segmentation approach presented in this article is twofold: (i) Whereas in the framework of statistical based active contour methods standard Shannon's entropy is most often considered as the region descriptor, we proposed an original fractional entropy measure inspired from Rényi's entropy making possible a relaxation of the sensibility of the descriptors to strong variations of the shapes of the non parametrically estimated related PDF. The main motivation was to overcome the limitations of Shannon's entropy which appeared not adapted to our segmentation problem; (ii) An unsupervised cell nuclei segmentation method is proposed for single channel actin tagged acquisitions without any enhancement or denoising preprocessing of the considered images. First obtained results are very encouraging.

On the theoretical aspect of this work, the possibility to locally relate the optimal choice of α parameter with the level of noise and/or the type of texture characterizing the image to

Annals of the BMVA Vol. 2013, No. 5, pp 1–15 (2013)

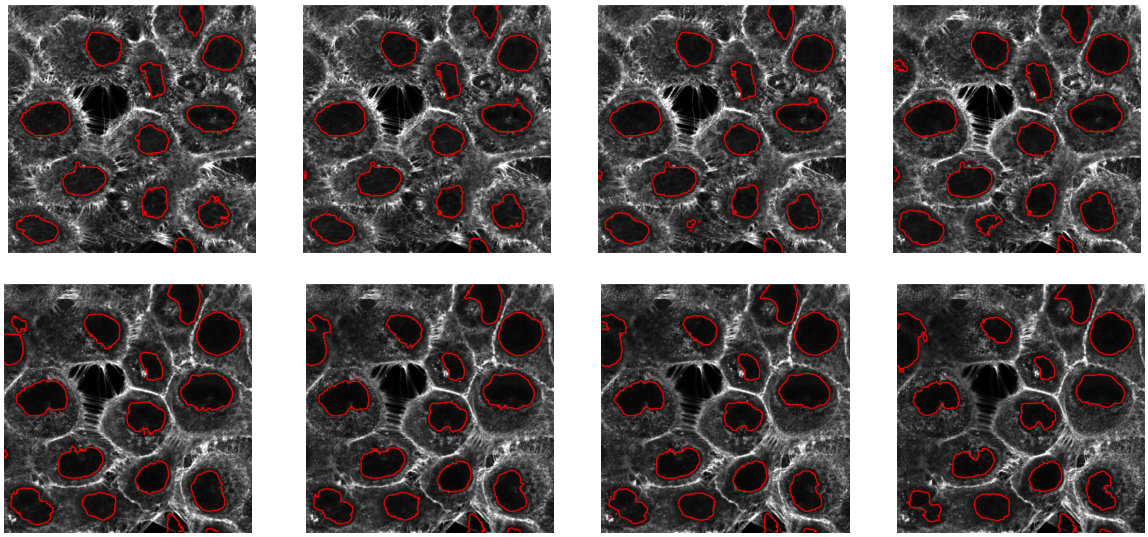

Figure 11: Segmentation of nuclei made on upper (upper row) and lower (bottom row) slices of the stack, mid-slice of Fig. 9 being the initialization level). $\alpha = 0.5$ and $g = 10$.

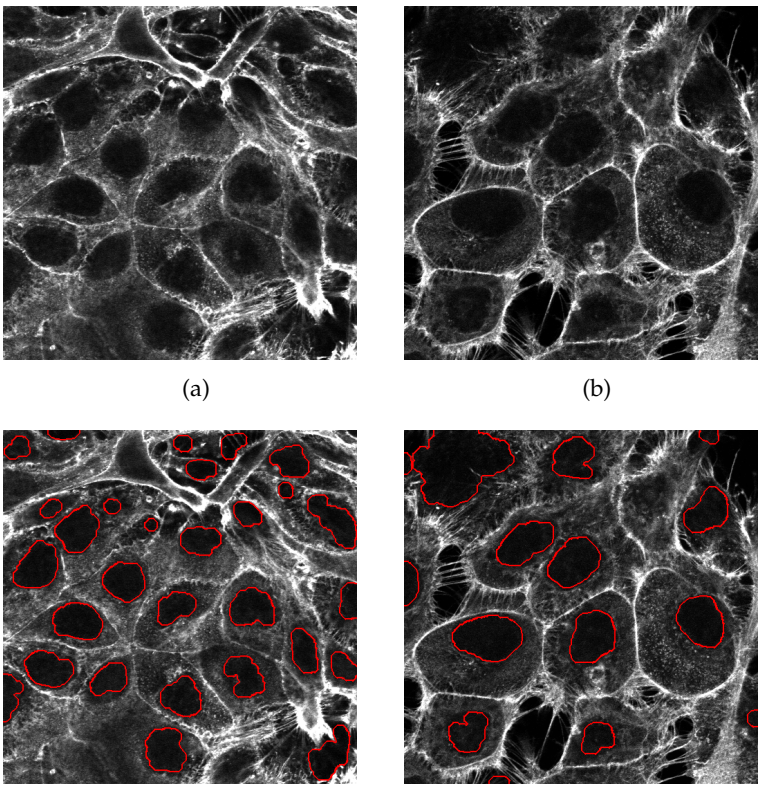

(a) (b)

(c) (d)

Figure 12: Segmentation of nuclei made on images extracted from different acquisitions. Up: original images, below: segmentation results with $\alpha = 0.5$ and $g = 1$.

segment remains a real challenge. From an application point of view, membrane segmentations will be the next step in order to have a complete segmentation of the cell structure.

Acknowledgements

This work was supported by the UK Engineering and Physical Sciences Research Council [TeRaFS project, grant number EP/H024913/1].

References

I. A. Ahmad and P. E. Lin. A nonparametric estimation of the entropy for absolutely continuous distributions. *IEEE Trans. Information Theory*, 1976.

G. Aubert, M. Barlaud, O. Faugeras, and S. Jehan-Besson. Image segmentation using active contours: Calculus of variations or shape gradients? *SIAM Journal on Applied Mathematics*, 63:2128–2154, June 2003.

P.A. Bromiley, N.A. Thacker, and E. Bouhova-Thacker. Shannon entropy, renyi entropy, and information. Technical report, School of Cancer and Imaging Sciences, University of Manchester, 2004.

T. F. Chan and L. A. Vese. Active contours without edges. *IEEE transactions on Image Processing*, 10(2):266–277, February 2001.

A. Hall. *The cytoskeleton and cancer*, volume 28. Springer Netherlands, Philadelphia, PA, USA, 06 2009. ISBN 0167-7659.

A. Herbulot, S. Jehan-Besson, S. Duffner, M. Barlaud, and G. Aubert. Segmentation of vectorial image features using shape gradients and information measures. *Journal of Mathematical Imaging and Vision*, 25(3):365–386, 2006.

S. Jehan-Besson, M. Barlaud, and G. Aubert. Deformable regions driven by an eulerian accurate minimization method for image and video segmentation. *Int. J. Comput. Vision*, 53:45–70, June 2003. ISSN 0920-5691.

M. Kass, A Witkin, and D. Terzopoulos. Snakes: Active contour models. *Int. J. Comput. Vision*, V1(4):321–331, January 1988.

F. Lecellier, M.J. Fadili, S. Jehan-Besson, G. Aubert, M. Revenu, and E. Saloux. Region-based active contours with exponential family observations. *Journal of Mathematical Imaging and Vision*, 36(1):28–45, January 2010.

B. Matuszewski, M. Murphy, D.R. Burton, T. Marchant, C. Moore, A. Histace, and F. Precioso. Segmentation of Cellular Structures in Actin Tagged Fluorescence Confocal Microscopy Images. In *Proceedings of IEEE International Conference on Image Processing*, pages 3142–3145, Brussels, Belgium, September 2011.

L. Meziou, A. Histace, F. Precioso, B. Matuszewski, and M. Murphy. Confocal Microscopy Segmentation Using Active Contour Based on Alpha-Divergence. In *Proceedings of IEEE ICIP conference*, pages 3138–3141, 09 2011.

L. Meziou, A. Histace, and F. Precioso. Alpha-divergence maximization for statistical region-based active contour segmentation with non-parametric PDF estimations. In *Proceedings of 37th IEEE International Conference on Accoustics, Speech and Signal Processing (ICASSP'12)*, pages 861–864, Kyoto, Japan, March 2012a.

L. Meziou, A. Histace, F. Precioso, B. Matuszewski, and F. Carreiras. Fractional Entropy Based Active Contour Segmentation of Cell Nuclei in Actin-Tagged Confocal Microscopy Images. In *Proceedings of the 16th conference on Medical Image Understanding and Analysis (MIUA)*, pages 117–129, Swansea, UK, July 2012b.

K. Mosaliganti, A. Gelas, A. Gouaillard, R. Noche, N. Obholzer, and S. Megason. Detection of spatially correlated objects in 3d images using appearance models and coupled active contours. In *Proceedings of MICCAI*, pages 641–648, London, UK, 2009. Springer-Verlag. ISBN 978-3-642-04270-6. doi: http://dx.doi.org/10.1007/978-3-642-04271-3_78. URL `http://dx.doi.org/10.1007/978-3-642-04271-3_78`.

C. Ortiz De Solorzano, E. Garcia Rodriguez, A. Jones, D. Pinkel, J. W. Gray, D. Sudar, and S. J. Lockett. Segmentation of confocal microscope images of cell nuclei in thick tissue sections. *Journal of Microscopy*, 193(3):212–226, 1999.

S. Osher and J. A. Sethian. Fronts propagating with curvature dependent speed: Algorithms based on hamilton-jacobi formulations. *Journal of Comp. Phy.*, 79:12–49, 1988.

S. Pop, A. Dufour, and J-C. Olivo-Marin. Image filtering using anisotropic structure tensor for cell membrane enhancement in 3d microscopy. In *Proceedings of IEEE-ICIP*, pages 2085–2088, September 2011.

A. Rényi. On measures of entropy and information. *4th Berkeley Symposium on Mathematical Statistics and Probability.*, 1:547–561, 1960.

A. Sarti, C. Ortiz De Solorzano, S. Lockett, and R. Malladi. A geometric model for 3d confocal microscope image analysis. *IEEE Transactions on Biomedical Engineering*, 47:1600–1609, 2000.

A. Sarti, R. Malladi, and J. A. Sethian. Subjective surfaces: A geometric model for boundary completion. *International Journal on Computer Vision*, 46(3):201–221, February 2002. ISSN 0920-5691.

J. Weickert, B. M. Ter Haar Romeny, and M. A. Viergever. Efficient and reliable schemes for nonlinear diffusion filtering. *IEEE trans. on IP*, 7(3):398–410, March 1998.

P. Yan, X. Zhou, M. Shah, and S. T. C. Wong. Automatic segmentation of high throughput rnai fluorescent cellular images. *IEEE Transactions on Information Technology in Biomedicine*, 12(1):109–117, January 2008.

C. Zanella, M. Campana, B. Rizzi, C. Melani, G. Sanguinetti, P. Bourgine, K. Mikula, N. Peyriéras, and A. Sarti. Cells segmentation from 3d confocal images of early zebrafish embryogenesis. *IEEE transactions on Image Processing*, 19(3):770–781, March 2010. ISSN 1057-7149.